

The Imprint of the Cosmic Dark Ages on the Near Infrared Background

R. Salvaterra¹ & A. Ferrara²

¹*SISSA, Via Beirut 4, 34100, Trieste, Italy*

²*Osservatorio Astrofisico di Arcetri, L.go E. Fermi 5, 50125 Firenze, Italy*

16 September 2018

ABSTRACT

The redshifted light of the first (Pop III) stars might substantially contribute to the near infrared background (NIRB). By fitting recent data with models including up-to-date Pop III stellar spectra, we find that such stars can indeed account for the whole NIRB residual (i.e. after ‘normal’ galaxy contribution subtraction) if the high redshift star formation efficiency is $f_{\star} = 10\% - 50\%$, depending on the IMF (the top-heaviest requiring lowest efficiency) and on the unknown galaxy contribution in the L band (our models, however, suggest it to be negligible). Such epoch of Pop III star formation ends in all models by $z_{end} \approx 8.8$, with a hard limit $z_{end} < 9$ set by J band observations. To prevent an associated IGM over-enrichment with heavy elements compared to observed levels in the IGM, pair-instability supernovae must be the dominant heavy element sources. Alternative explanations must break the light-metal production link by advocating very massive stars ($M > 260M_{\odot}$) locking their nucleosynthetic products in the compact remnant or by postulating an extremely inhomogeneous metal enrichment of the Ly α forest. We discuss these possibilities in detail along with the uncertainties related to the adopted zodiacal light model.

Key words: galaxies: formation - intergalactic medium - black holes - cosmology: theory

1 INTRODUCTION

The cosmic infrared background (CIRB) can set important constraints on the star formation history of the universe (e.g. Hauser & Dwek 2001 and references therein). The CIRB consists of the cumulative radiation from all extragalactic sources. In the near-infrared (NIR) the CIRB is dominated by starlight, whereas in the mid- and far-infrared it results from dust emission.

Different authors had provided measures of the Near Infrared Background (NIRB) in the J, K, and L bands using the data of DIRBE instrument aboard of COBE satellite. Recently, Matsumoto et al. (2000) have accurately measured the NIRB from 1.4 to 4 μm , using the data taken with the Near Infrared Spectrometer. The largest uncertainty on the NIRB measurements is due to the subtraction of the interplanetary dust (IPD) scattered sunlight. In spite of this difficulty some studies have concluded that normal galaxies cannot account for the whole observed NIRB (Totani et al. 2001).

Bond, Carr & Hogan (1986) pointed out that the first population of zero-metallicity stars, the so called Population III (Pop III), might contribute to the cosmic background in the near infrared. More recently, Santos, Bromm

& Kamionkowski (2001) suggested that a significant part of the unaccounted NIRB could come from Pop III stars. They considered a very top-heavy Initial Mass Function (IMF), assuming that all stars have masses $\gtrsim 300 M_{\odot}$ as recent three-dimensional numerical simulations seem to suggest (Bromm, Coppi & Larson 1999, 2002; Abel, Bryan & Norman 2000). In this paper we improve on these earlier studies in many respects. First, we confront theoretical predictions with the recent Matsumoto et al. (2000) data, which provides a much tighter test and constraint. Secondly, we consider the effect of several IMFs. Third, we use the new stellar spectra of Schaerer (2002) for zero age mean sequence (ZAMS) metal free stars, including the nebular continuous emission found to be very important for stars with strong ionizing fluxes.

We fit the estimate of the unaccounted NIRB finding limits on the star formation efficiency and on the redshift at which the formation of Pop III stars ends. We compare our results with high redshift observations and draw some results on IGM metal enrichment due to Pop III supernovae.

The paper is organized as follows: in §2 we describe the background intensity calculation, the stellar spectra used, and how we model the IGM. In §3 the available data in the NIR range are reviewed along with the number counts

arXiv:astro-ph/0210331v1 15 Oct 2002

of normal galaxies from deep field surveys. We discuss the results of our analysis in §4; in §5 we present our conclusions.

We adopt the ‘concordance’ model values for the cosmological parameters: $h = 0.7$, $\Omega_M = 0.3$, $\Omega_\Lambda = 0.7$, $\Omega_b = 0.038$, $\sigma_8 = 0.9$, and $\Gamma = 0.21$. Here h is the dimensionless Hubble constant, $H_0 = 100h \text{ km s}^{-1} \text{ Mpc}^{-1}$; Ω_M , Ω_Λ , and Ω_b are the total matter, cosmological constant, and baryon density in units of the critical density; σ_8 gives the normalization of the power spectrum on $8h^{-1} \text{ Mpc}$ scale and Γ is the shape of the power spectrum. We use the power spectrum for the fluctuations derived by Efstathiou, Bond & White (1992).

2 COSMIC INFRARED BACKGROUND

The mean specific intensity of the background $I(\nu_0, z_0)$, as seen at frequency ν_0 by an observer at redshift z_0 , is given by

$$I(\nu_0, z_0) = \frac{1}{4\pi} \int_{z_0}^{\infty} \epsilon(\nu, z) e^{-\tau_{eff}(\nu_0, z_0, z)} \frac{dl}{dz} dz \quad (1)$$

(Peebles 1993). Here $\epsilon(\nu, z)$ is the comoving specific emissivity, $\nu = \nu_0(1+z)/(1+z_0)$, $\tau_{eff}(\nu_0, z_0, z)$ is the effective optical depth at ν_0 of the IGM between redshift z_0 and z , and dl/dz is the proper line element

$$\frac{dl}{dz} = c[H_0(1+z)E(z)]^{-1},$$

where c is the light speed and

$$E(z) = [\Omega_M(1+z)^3 + \Omega_\Lambda + (1 - \Omega_M - \Omega_\Lambda)(1+z)^2]^{1/2}. \quad (2)$$

2.1 The Comoving Specific Emissivity

The gas initially virialized in the potential well of the parent dark matter halo, can subsequently fragment and ignite star formation only if the gas can cool efficiently and lose pressure support. For a plasma of primordial composition at temperature $T < 10^4 \text{ K}$, the typical virial temperatures of the early bound structures, the only efficient coolant is molecular hydrogen. Thus, a minimum H_2 fraction is required for a gas cloud to be able to cool in a Hubble time. As the intergalactic relic H_2 abundance falls short by at least two orders of magnitude such requirement, the fate of a virialized lump depends crucially on its ability to rapidly increase its H_2 content during the collapse phase. Once a critical H_2 fractional abundance of $\sim 5 \times 10^{-4}$ is achieved in an object, the lump will cool, fragment and eventually form stars. This criterion is met only by larger haloes, so that for each virialization redshift there will exist a critical mass, $M_{min}(z)$, for which protogalaxies with total mass $M_h > M_{min}$ form stars and those with mass $M_h < M_{min}$ do not. We adopt here $M_{min}(z)$ as computed by Fuller & Couchman (2000).

In absence of additional effects that could prevent or delay the collapse, we can associate to each dark matter halo with mass $M_h > M_{min}$ a corresponding stellar mass

$$M_\star = f_\star \frac{\Omega_b}{\Omega_M} M_h, \quad (3)$$

where f_\star is the fraction of baryons able to cool and form stars; we will refer to this quantity as the star formation efficiency. Thus, the stellar mass per unit comoving volume at redshift z contained in haloes with mass $M_h > M_{min}(z)$ is given by

$$\rho_\star(z) = \int_{M_{min}(z)}^{\infty} n(M_h, z) M_\star dM_h, \quad (4)$$

where $n(M_h, z)$ is the comoving number density of dark matter haloes of mass M_h at redshift z given by Press & Schechter (1974).

The comoving specific emissivity, in units of $\text{erg s}^{-1} \text{ Hz}^{-1} \text{ cm}^{-3}$, is then

$$\epsilon(\nu, z) = l_\nu(z) \rho_\star(z), \quad (5)$$

where $l_\nu(z)$ is the specific luminosity of the population [in $\text{erg s}^{-1} \text{ Hz}^{-1} M_\odot^{-1}$] at redshift z (see Sec. 2.4).

2.2 The Intergalactic Medium

Absorption due to intergalactic gas located in discrete systems along the line of sight can seriously distort our view of objects at cosmological distances. At wavelengths shortward of $\text{Ly}\alpha$ ($\lambda < 1216 \text{ \AA}$) in the emitter rest frame, the source continuum intensity is attenuated by the combined blanketing of lines in the Lyman series, and strongly suppressed by the continuum absorption from neutral hydrogen shortward of the Lyman limit in the emitter rest frame. As pointed out by Haiman & Loeb (1999) no flux is transmitted at wavelengths $\lambda_0 < \lambda_\alpha(1+z_s)$ from sources at redshift $1+z_s > 32/27(1+z_i)$, where $z_i = 6.2$ (Gnedin 2001) is the currently favored reionization redshift.

The effective optical depth τ_{eff} through the IGM is defined as $e^{-\tau_{eff}} = \langle e^{-\tau} \rangle$, where the mean is taken over all the lines of sight to the redshift of interest. For a Poisson distribution of absorbers (Madau 1991, 1992),

$$\tau_{eff}(\nu_0, z_0, z) = \int_{z_0}^z dz' \int_0^\infty dN_{\text{HI}} \zeta(N_{\text{HI}}, z') (1 - e^{-\tau}), \quad (6)$$

where $\zeta(N_{\text{HI}}, z')$ is the distribution of the absorbers as a function of redshift and neutral hydrogen column density, N_{HI} ; $\tau(\nu')$ is the optical depth of an individual cloud for ionizing radiation at frequency ν' .

For the Lyman- α forest, in the wavelength range $\lambda_\beta < \lambda_0/(1+z_{em}) < \lambda_\alpha$ where $\lambda_\alpha = 1216 \text{ \AA}$ and $\lambda_\beta = 1026 \text{ \AA}$, we have (Madau 1995)

$$\tau_{eff} = 0.0036 \left(\frac{\lambda_0}{\lambda_\alpha} \right)^{3.46}.$$

When $\lambda_0/(1+z_{em}) < \lambda_\beta$, a significant contribution to the blanketing opacity comes from the higher order lines of the Lyman series. In the wavelength range $\lambda_{i+1} < \lambda_0/(1+z) < \lambda_i$, the total effective line-blanketing optical depth can be written as the sum of the contributions from the $j \rightarrow 1$ transitions,

$$\tau_{eff} = \sum_{j=2,i} A_j \left(\frac{\lambda_0}{\lambda_j} \right)^{3.46}, \quad (7)$$

j	λ_j [Å]	A_j
2	1216	3.6×10^{-3}
3	1026	1.7×10^{-3}
4	973	1.2×10^{-3}
5	950	9.3×10^{-4}

Table 1. Coefficients A_j corresponding to λ_j in eq. 7

N_{HI}	A	β	γ
$< 10^{14}$	1.45×10^{-1}	1.40	2.58
$10^{14} - 10^{16}$	6.04×10^{-3}	1.86	2.58
$10^{16} - 10^{19}$	2.58×10^{-2}	1.23	2.58
$10^{19} - 10^{22}$	8.42×10^{-2}	1.16	1.30

Table 2. Best fit value (Model A1) for A , β and γ (Fardal et al. 1998) used in eq. 9

where λ_j and the corresponding values for A_j are given in Table 1.

Continuum absorption from neutral hydrogen along the line of sight affects photons observed at $\lambda_0/(1+z_{em}) < \lambda_L$, where $\lambda_L = 912 \text{ \AA}$ is the Lyman limit. We have

$$\tau = N_{\text{HI}} \sigma \quad (8)$$

where $\sigma(\lambda_0, z) \sim 6.3 \times 10^{-18} (\lambda_0/\lambda_L)^3 (1+z)^{-3} \text{ cm}^2$ (Osterbrock 1989) is the hydrogen photoionization cross section, and $(1+z_c) = (\lambda_0/\lambda_L)$ for $\lambda_0 > \lambda_L$, whereas for $\lambda_0 < \lambda_L$, HI absorbs photons all the way down to $z_c = 0$.

For the redshift and column density distribution of absorption lines, the usual form can be adopted

$$\zeta(N_{\text{HI}}, z) = \left(\frac{A}{10^{17}} \right) \left(\frac{N_{\text{HI}}}{10^{17} \text{ cm}^{-2}} \right)^{-\beta} (1+z)^\gamma. \quad (9)$$

where the values of coefficients A , β and γ in different ranges in N_{HI} are given in Table 2, and are taken from Fardal, Giroux & Shull (1998).

2.3 Scattering of Ly α Photons

Ly α line photons from first galaxies are absorbed by neutral hydrogen along the line of sight (Gunn & Peterson 1965). However, they are not destroyed but scatter and diffuse in frequency to the red of the Ly α resonance owing to the Hubble expansion of the surrounding HI. Eventually, when their net frequency shift is sufficiently large, they escape and travel freely toward the observer. The profile results in a strong, asymmetric Ly α emission line around 1225 Å with a scattering tail extending to long wavelengths.

The resulting scattered line profile, $\Phi(\nu, z)$, has been simulated by Loeb & Rybicki (1999). Here, we use the fitting analytical expression given by Santos et al. (2001)

$$\Phi(\nu, z) = \begin{cases} \nu_*(z) \nu^{-2} \exp\left[-\frac{\nu-\nu_*}{\nu}\right] & \text{if } \nu > 0 \\ 0 & \text{if } \nu \leq 0 \end{cases}, \quad (10)$$

$$\nu_*(z) = 1.5 \times 10^{12} \text{ Hz} \left(\frac{\Omega_b h^2}{0.019} \right) \left(\frac{h}{0.7} \right)^{-1} \frac{(1+z)^3}{E(z)}, \quad (11)$$

where $E(z)$ is defined in eq. (2). Note that we have allowed the IGM in the vicinity of the emitting galaxy to be overdense by a factor $\delta \approx 10$, to account for the high clustering of first sources.

2.4 Emission from a Pop III ‘Stellar Cluster’

We calculate the emission of a Pop III ‘stellar cluster’ according to the equation:

$$l_\nu(z) = \int_{M_l}^{M_u} F(\nu, M, z) \phi(M) dM, \quad (12)$$

where $\phi(M)$ is the IMF normalized so that $\int_{M_l}^{M_u} \phi(M) dM = 1$; M_l and M_u are the lower and upper mass limits. The spectrum of a star of mass M at the rest-frame frequency ν and redshift z is given by

$$F(\nu, M, z) = l_\nu^{star}(M) + l_\nu^{neb}(M) + l_\nu^{Ly\alpha}(M, z). \quad (13)$$

where $l_\nu^{star}(M)$ is the spectrum of a Pop III star of mass M , l_ν^{neb} is the emission of the nebula surrounding the star, and $l_\nu^{Ly\alpha}(z)$ is the emission due to Ly α line photons from a source at redshift z scattered by the IGM (see Sec. 2.3).

As spectra of Pop III we adopt here those modeled by Schaerer (2002) who relaxed some assumptions made in previous works (Tumlinson & Shull 2000; Tumlinson, Giroux & Shull 2001; Bromm, Kudritzki, & Loeb 2001). Schaerer (2002) presented realistic models for massive Pop III stars and stellar populations based on non-LTE atmospheres, recent stellar evolution tracks and up-to-date evolutionary synthesis models. Moreover, he included nebular continuous emission, which cannot be neglected for metal-poor objects with strong ionizing fluxes. This process increases significantly the total continuum flux at wavelengths redward of Lyman- α and leads in turn to reduced emission line equivalent widths.

We add thus the contribution of the nebular emission ($n_e = 100 \text{ cm}^{-3}$ is assumed) as described in Schaerer (2002):

$$l_\nu^{neb} = \frac{\gamma_{tot}}{\alpha_B} (1 - f_{esc}) q(H) \quad (14)$$

(e.g. Osterbrock 1989), where α_B (in units of $\text{cm}^{-3} \text{ s}^{-1}$) is the Case B recombination coefficient for hydrogen and f_{esc} is the ionizing photon escape fraction out of the idealized region considered here (we assume $f_{esc} = 0$); $q(H) = Q(H)/M$, where $Q(H)$ is the ionizing photon rate (in units of s^{-1}) for H and is given for different stellar masses in Table 3 of Schaerer (2002). The continuous emission coefficient γ_{tot} , including free-free and free-bound emission by H, neutral He and single ionized He, as well as the two-photon continuum of hydrogen is given by

$$\gamma_{tot} = \gamma_{HI} + \gamma_{2q} + \gamma_{HeI} \frac{n(He^+)}{n(H^+)} + \gamma_{HeII} \frac{n(He^{++})}{n(H^+)}. \quad (15)$$

The continuous emission coefficients γ_i (in units of $\text{erg cm}^3 \text{ s}^{-1} \text{ Hz}^{-1}$) are taken from Aller (1987) for an electron temperature of 20000 K. The spectrum of a 1000 M_\odot star (with and without the nebular emission) and of a 5 M_\odot star are plotted in Fig. 1.

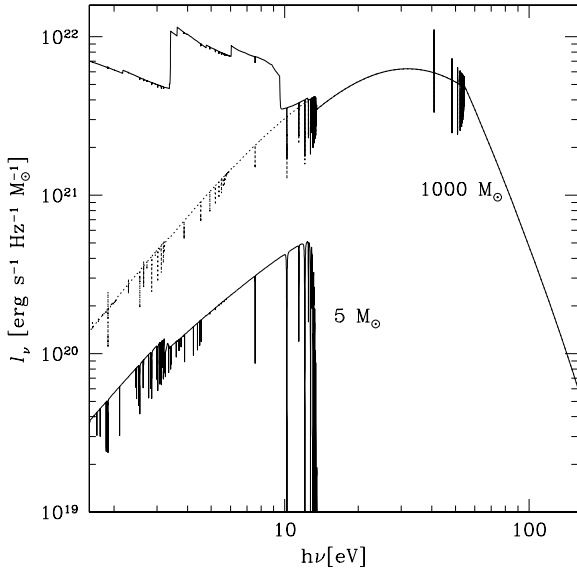


Figure 1. Spectra of individual Pop III stars plotted as luminosity per unit of stellar mass (in $\text{erg s}^{-1} \text{Hz}^{-1} M_\odot^{-1}$) vs. energy (in eV). The spectrum of a $1000 M_\odot$ star with (solid line) and without (dashed) nebular emission and of a $5 M_\odot$ are shown. For the $5 M_\odot$ star the contribution of the nebular emission is negligible.

Finally, the emission of Ly α line photons is given by

$$l_\nu^{Ly\alpha}(z) = c_{Ly\alpha}(1 - f_{esc})q(H)\Phi(\nu_{Ly\alpha} - \nu, z), \quad (16)$$

where $c_{Ly\alpha} = 1.04 \times 10^{-11}$ erg (Schaerer 2002). The line profile $\Phi(\nu)$ is given in eq. (10).

2.4.1 Initial Mass Function

The issue of the mass distribution of first metal free stars has been tackled via various hydrodynamical models and other studies (e.g. Abel et al. 1998, Bromm et al. 1999, 2001, 2002, Nakamura & Umemura 2001, Ripamonti et al. 2002). There seems to be an overall consensus that massive stars (up to $1000 M_\odot$) may form. Simulations seem to suggest that the primordial IMF might have been biased towards stellar masses $\geq 100 M_\odot$, but other studies (e.g. Nakamura & Umemura 2001) found that the formation of stars with masses down to $1 M_\odot$ is not excluded.

In the local universe the IMF is usually well described by the standard Salpeter law (Salpeter 1955)

$$\phi(M) \propto M^{-2.35}. \quad (17)$$

Larson (1998) suggested a different form for the high z IMF. This has a universal Salpeter-like form at the upper end, but flattens below a characteristic mass, M_c which may vary with time. By increasing M_c we can mimick a top-heavy IMF of Pop III stars,

$$\phi(M) \propto M^{-1} \left(1 + \frac{M}{M_c}\right)^{-1.35}. \quad (18)$$

Hernandez & Ferrara (2001) have explored the predictions of the standard hierarchical clustering scenario of galaxy formation, regarding the numbers and metallicities of Pop III stars that are likely to be found within our Galaxy

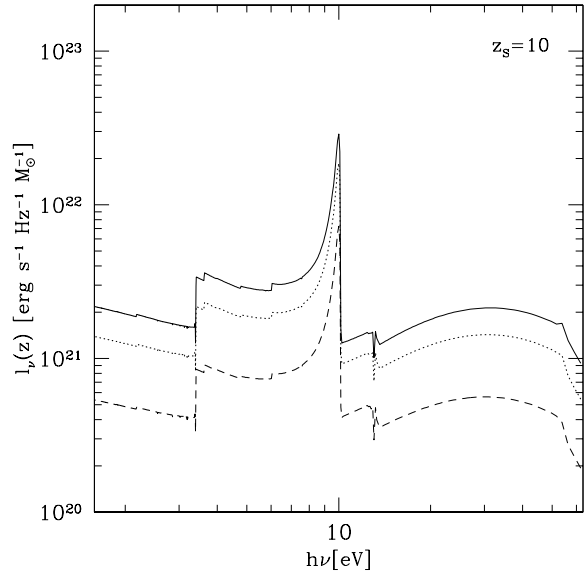


Figure 2. Pop III stellar cluster spectra for different IMFs. Dashed line: Salpeter. Dotted line: heavy IMF. Solid line: very heavy IMF. The sharp peak around 1220 \AA is due to Ly α nebular emission for sources at $z_s = 10$, filtered through the IGM. The flux at $E > 13.6$ eV is then strongly suppressed by the absorption due to the intergalactic gas (see Sec. 2.2)

today. By comparing these values with observational data, they suggested that the IMF of first stars was increasingly high-mass weighted towards high redshifts, levelling off at $z \geq 9$ at a characteristic stellar mass scale of $10\text{-}15 M_\odot$.

In view of our poor knowledge of the IMF at high redshift we consider here three different distributions of mass for the first population of stars: Salpeter, Larson with $M_c = 15 M_\odot$ (heavy IMF), and Larson with $M_c = 100 M_\odot$ (very heavy IMF). For all IMFs, $M_l = 1 M_\odot$ and $M_u = 1000 M_\odot$. In Fig. 2 are shown the resulting spectra of a Pop III cluster at redshift $z_s = 10$ for the three different IMFs assumed.

3 OBSERVATIONAL CONSTRAINTS

Observations of the NIRB are seriously hampered by the strong atmospheric foreground (e.g. Mandolesi et al. 1998). On the other hand space measurements are not easy because it is difficult to subtract correctly the contribution to the extragalactic background light by interplanetary dust scattered sunlight (zodiacal light). Using the data from the instrument DIRBE aboard of the COBE satellite and from the 2MASS data, Cambresy et al. (2001) found a non zero, isotropic background in the J and K bands. With the same data but a different zodiacal light model, Wright & Johnson (2001) extended the flux estimate to the L band. Cambresy's and Wright's results in the J and K bands are compatible if the same zodiacal light model is applied. Matsumoto et al. (2000) provided a preliminary analysis of the the NIRS data obtaining a detection of the NIRB in the $1.4\text{-}4 \mu\text{m}$ range. They applied the same zodiacal light model of Cambresy et

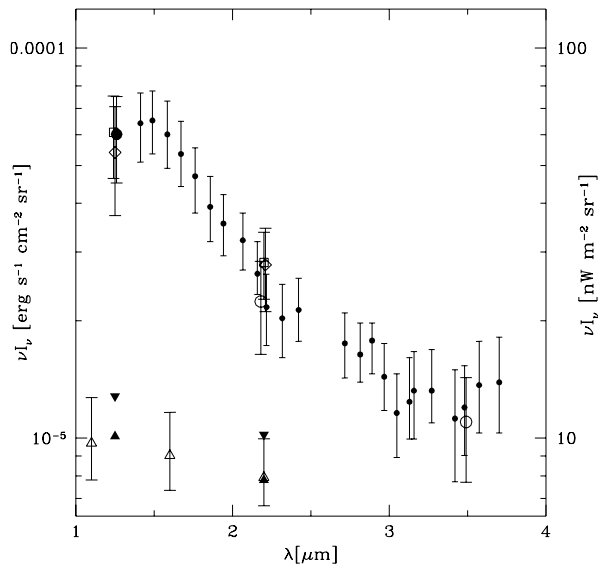


Figure 3. Available NIR data. The small filled circles are the NIRS data (Matsumoto et al. 2000). The open symbols are the DIRBE results: squares for Wright (2001), diamonds for Cambresy et al. (2001), and circles for Gorjian, Wright & Chary (2000). The big filled circle is the Kiso star count measurement. The data are slightly offset for clarity. The errors are at 1σ and for all the data the Kelsall et al. (1998) model for the zodiacal light is applied. The open triangles are the count integration from the *Hubble Deep Field* (Madau & Pozzetti 2000), whereas the filled triangles report upper and lower limits on the count integration from *Subaru Deep Field* when also the contribution of missed galaxies is considered (Totani et al. 2001).

al. (2001) and obtained compatible results in the DIRBE bands. At 8000 \AA , Bernstein, Freedman & Madore (2002) observed a CIRB of $1.76 \pm 0.48 \times 10^{-5} \text{ erg s}^{-1} \text{ cm}^{-2} \text{ sr}^{-1}$, that is ~ 4 times smaller than the DIRBE and NIRS measurements in the J band, showing a break around $\sim 1 \mu\text{m}$. The integrated counts in the J and K bands from deep surveys do not account for the total NIRB (Madau & Pozzetti 2000; Totani et al. 2001). Totani et al. (2001) modeled the contribution of galaxies missed by deep galaxy surveys. They found unlikely that the contribution of all the normal galaxies to the NIRB is larger than 30%. All the available data are plotted in Fig. 3. In Table 3 the estimate of the NIRB from the DIRBE data (top panel) and the contribution of normal galaxies (bottom panel) are reported.

3.1 The DIRBE Data

The Diffuse Infrared Background Experiment (DIRBE) on board of the Cosmic Background Explorer (COBE, see Boggess et al. (1992)) satellite was designed to search for the Cosmic Infrared Background from $1.25 \mu\text{m}$ to $240 \mu\text{m}$. The DIRBE instrument (Silverberg et al. 1993) was an absolute photometer which provided maps of the full sky in 10 broad bands at $1.25, 2.2, 3.5, 4.9, 12, 25, 60, 100, 140,$ and $240 \mu\text{m}$ with a starlight rejection of $< 1 \text{ nW m}^{-2} \text{ sr}^{-1}$ and an absolute brightness calibration uncertainty of 0.05 and $0.03 \text{ nW m}^{-2} \text{ sr}^{-1}$, at $1.25 \mu\text{m}$ and $2.2 \mu\text{m}$ respectively.

A summary of the DIRBE results is provided by Hauser et al. (1998) and all the NIRB measures based on the DIRBE data are reported in Table 3 (top panel).

In the near infrared bands the dominant foreground intensities in the DIRBE data are the zodiacal light and the light from stars in the Milky Way.

A first attempt to detect the NIRB from the DIRBE data was carried out by the DIRBE group but this gave only an upper limit and failed the tests of isotropy even in limited regions of sky (Arendt et al. 1998). Dwek & Arendt (1998) made a correlation study for the K and L bands and obtained a lower limit for the L band.

Gorjian et al. (2000) removed the foreground due to Galactic stars by directly measuring all stars brighter than 9th magnitude at 2.2 and $3.5 \mu\text{m}$ in a $2^\circ \times 2^\circ$ dark spot near the North Galactic Pole using ground-based telescopes. They calculated the contribution of fainter stars using the statistical model of Wainscoat et al. (1992) and subtracted the zodiacal light contribution using an improvement of the Wright (1998) model. Gorjian et al. found significant positive residuals in the K and L bands which they identified as a probable detection of the NIRB. Wright & Reese (2000) obtained a consistent estimate of the NIRB in the same bands using a different approach based on a histogram fitting method to remove the stellar foreground from the DIRBE data.

Wright (2001) used the Two Micron All Sky Survey (2MASS) data (Cutri et al. 2000) to remove the contribution of Galactic stars brighter than 14th magnitude from the DIRBE maps at 1.25 and $2.2 \mu\text{m}$ in four dark regions in the north and south Galactic Pole caps. For the subtraction of the zodiacal light foreground the model presented in Gorjian et al. (2000) is applied. Cambresy et al. (2000) have also used the 2MASS data to remove the Galactic stars from the DIRBE data, but they modeled the zodiacal light as in Kelsall et al. (1998). Their results agree with those of Wright (2001) if the same zodiacal light model is applied.

Recently, Wright & Johnson (2001) extended the analysis of Wright (2001) to 13 fields with a wide range of ecliptic latitudes tripling the number of pixels. They obtained an estimate of the NIRB at 1.25 and $2.2 \mu\text{m}$ consistent with the previous results. They also found a significant residual in the L band combining the Wright (2001) and Dwek & Arendt (1998) techniques, consistent with the Wright & Reese (2000) result.

Matsumoto et al. (in preparation) observed in the J band with the Kiso Schmidt Telescope toward the DIRBE dark spot. They subtracted all detected stars brighter than 14th magnitude and estimated the contribution of fainter stars by the Cohen’s sky model (Cohen 1997). They used the Kelsall’s zodiacal light model.

3.2 The NIRS Data

The Near Infrared Spectrometer (NIRS)* is one of the focal instruments of the InfraRed Telescope in Space (IRTS) (Noda et al. 1994). The NIRS covers the wavelength range from 1.4 to $4.0 \mu\text{m}$ with a spectral resolution of $0.13 \mu\text{m}$. The beam size is $8' \times 20'$, which is considerably smaller than

* <http://www.ir.isas.ac.jp/irts/nirs/index-e.html>

J band (1.25 μm)	K band (2.2 μm)	L band (3.5 μm)	M	Reference
	(16.2 \pm 6.4) 22.4 \pm 6.0	11.0 \pm 3.3	W K	Gorijan et al. 2000
	(23.1 \pm 5.9)	(12.4 \pm 3.2)	W	Wright & Reese 2000
(27.7 \pm 14.5) 60.8 \pm 14.5	(19.9 \pm 5.3) 28.2 \pm 5.5		W K	Wright 2001
54.0 \pm 16.8	27.8 \pm 6.7		K	Cambresy et al. 2001
(24.3 \pm 18)	(24 \pm 6)	(13.8 \pm 3.4)	W	Wright & Johnson 2001
60.1 \pm 15			K	Kiso star counts
Simple Integration of Observed Galaxy Counts				
(9.7 $^{+3.0}_{-1.9}$) ^a 10.9 \pm 1.1	7.9 $^{+2.0}_{-1.2}$ 8.3 \pm 0.8			Madau & Pozzetti 2000 Totani et al. 2001
Estimated Resolved Fraction				
0.97 0.95	0.93 0.92			Model A Model B
Contribution to the NIRB of All Normal Galaxy				
10.1-12.8	7.8-10.2			Totani et al. 2001

Table 3. Summary of the recent observations of the NIRB from the DIRBE data (top panel). Units are $\text{nWm}^{-2}\text{sr}^{-1}$ (or $10^{-6} \text{ erg s}^{-1} \text{ cm}^2 \text{ sr}^{-1}$). In the fourth column is given the Model used to subtract the Zodiacal Light: 'W' stands for Wright (1998) and 'K' is for Kelsall et al. (1998). In the bottom panel are shown the results of count integration from the *Hubble Deep Field* (Madau & Pozzetti 2000) and from the *Subaru Deep Field* (Totani et al. 2001) surveys, the estimate of the contribution of missed galaxies (Totani et al. 2001). Model A: number evolution with $\eta \sim 1$; Model B: no number evolution with $\eta = 0$) and the total flux from all normal galaxies (Totani et al. 2001).

^a Estimate at slightly different wavelengths

that of DIRBE; about 7% of the sky is surveyed. In order to reduce the contribution from the faint stars, the sky at high latitudes ($b > 40^\circ$) is chosen.

Matsumoto et al. (2000) provided a preliminary analysis of the NIRS data, reporting detection of the Cosmic Infrared Background based upon analysis of the five days of data which were least disturbed by atmospheric, lunar, and nuclear radiation effects. The sky area analyzed included Galactic latitudes from 40° to 58° , and ecliptic latitudes from 12° to 71° . NIRS is able to identify stars brighter than 10.5 mag. at 2.24 μm , whereas to find out the contribution of fainter stars the Cohen model (1997) is used. The model of Kelsall et al. (1998) is applied to subtract the contribution of the zodiacal light foreground, interpolating between the DIRBE wavelengths to the wavelengths of the NIRS measurements. After subtraction of the IPD contribution, there remains a fairly isotropic residual emission, which they interpreted as evidence for a non-zero background. To obtain a quantitative value for the background at each wavelength they correlated their star-subtracted brightness at each point with the IPD model brightness, and used the extrapolation to zero IPD contribution as a measurement of the NIRB.

The NIRB intensities reported by Matsumoto et al. (2000) near 2.2 and 3.5 μm are similar to the values found by Gorjian et al. (2000). At shorter wavelengths, the NIRS

results continue to rise steeply to $\sim 6.5 \times 10^{-5} \text{ erg s}^{-1} \text{ cm}^{-2} \text{ sr}^{-1}$ at 1.4 μm . This is somewhat above the 95% CL upper limit at 1.25 μm of Wright (2001), but it is in agreement with the value obtained by Cambresy et al. (2001) using the same zodiacal light model. The NIRS result implies an integrated background energy over the 1.4-4.0 μm range of $\sim 3.0 \times 10^{-5} \text{ erg s}^{-1} \text{ cm}^{-2} \text{ sr}^{-1}$.

The preliminary report by Matsumoto et al. (2000) does not provide details regarding systematic uncertainties in their results. The largest uncertainty in the reported NIRB values is attributed to the IPD model.

3.3 Galaxy Contribution from Deep Counts

Deep optical and NIR galaxy counts provide an estimate of the extragalactic background light (EBL) coming from normal galaxies in the universe. Madau & Pozzetti (2000) derived the contribution of known galaxies in the UBVI-JHK bands from the *Southern Hubble Deep Field*. Although the slope of the number-magnitude relation of the faintest counts is flat enough for the count integration to converge, the recent observations of the NIRB (see previous Section) suggest that the diffuse EBL flux is considerably larger than the count integration. However, a considerable fraction of EBL from galaxies could still have been missed in deep galaxy surveys because of various selection effects.

IMF	galaxy model	f_*		
		$z_{end} = 8$	$z_{end} = 9$	$z_{end} = 10$
Salpeter	cut	0.37 ± 0.03	0.59 ± 0.05	0.89 ± 0.08
	flat	0.24 ± 0.03	0.39 ± 0.05	0.58 ± 0.08
Heavy	cut	0.15 ± 0.01	0.24 ± 0.02	0.36 ± 0.03
	flat	0.10 ± 0.01	0.15 ± 0.02	0.23 ± 0.03
Very heavy	cut	0.10 ± 0.01	0.15 ± 0.01	0.23 ± 0.02
	flat	0.06 ± 0.01	0.10 ± 0.01	0.15 ± 0.02

Table 4. Values of f_* from the fit to the data with different IMFs. The quoted statistical errors are at 95% C.L..

Totani et al. (2001) using the *Subaru Deep Field* data (Maihara et al. 2001) have shown that more than 80%-90% of EBL from galaxies has been resolved in the K and J bands and that the contribution by missing galaxies cannot account for the discrepancy between the count integration and the NIRB observations. In Table 3 (bottom panel) we show the count integration in optical and NIR bands from Madau & Pozzetti (2000) and Totani et al. (2001), and the resolved fractions for two galaxy evolution models. The possible number evolution of galaxies is considered by a phenomenological model in which the Schechter parameters of the luminosity function have a redshift dependence as $\phi^* \propto (1+z)^\eta$ and $L^* \propto (1+z)^{-\eta}$; i.e., luminosity density is conserved. In Model A an evolution with $\eta = 1$ is considered, whereas in Model B no evolution ($\eta = 0$) is assumed (see Totani et al. (2001) for more details). Currently no measure of the contribution of normal galaxies to the NIRB in L band is available whose accurate measurement has to await for SIRTf.

4 MODEL VS. OBSERVATIONS

We compare the NIR data with the predictions of our model, summarized by eq. (1). The data set is composed by the measurements of Matsumoto et al. (2000) and those obtained by the DIRBE data using the Kelsall model for the zodiacal light emission as reported in Table 3 (top panel). For each wavelength we subtracted from the data the contribution of normal galaxies using the upper (lower) limits in the J and K band, obtained by Totani et al. (2001) (last line of Table 3). As discussed already, for $\lambda > 2.2 \mu\text{m}$ no estimate of the NIRB due to normal galaxies is available. Thus in the range 2.2 to 4 μm we consider two extreme cases: no contribution from normal galaxies (labeled with **cut**) and a constant contribution (labeled with **flat**).

4.1 Model Results

The fit results are quite sensitive to the adopted IMF and to the way we model the contribution of normal galaxies for $\lambda > 2.2 \mu\text{m}$. In Table 4 are reported the results of the fit for different IMFs, count integration model, and z_{end} . The reported errors represent the statistical uncertainty of the fit, but systematic uncertainties difficult to evaluate might be present. In Fig. 4 are plotted the values of the star formation efficiency and the corresponding χ^2/DOF (Degree of Freedom) as function z_{end} for the **cut** galaxy count model.

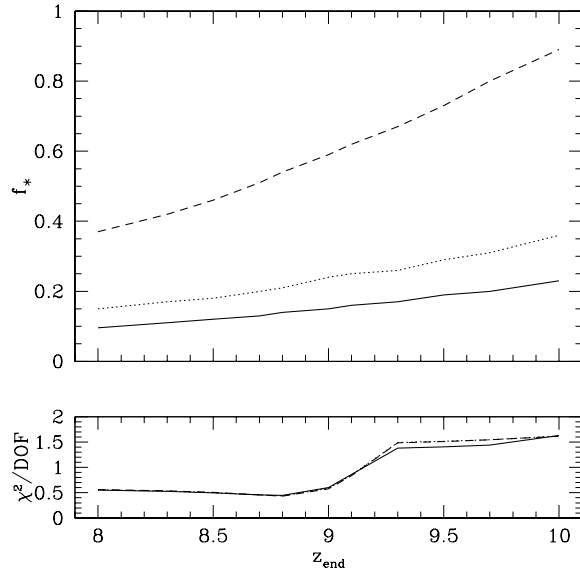


Figure 4. Star formation efficiency f_* accounting for the whole unexplained NIRB, as a function of redshift at which the formation of Pop III stars ends. The model **cut** for the counts integration for $\lambda > 2.2 \mu\text{m}$ is adopted. *Dashed line:* Salpeter IMF. *Dotted line:* heavy IMF. *Solid line:* very heavy IMF. The bottom panel shows the value of χ^2/DOF .

The χ^2 increases rapidly as z_{end} becomes greater than 9, showing that in this case our model fails to account of the NIRB observation in the J band.

For a Salpeter IMF we find that a large fraction of baryons have to be turned into stars to account of the whole unexplained NIRB. This fraction goes from 37% ($z_{end} = 8$) to 89% ($z_{end} = 10$) if we consider the case of no contribution from normal galaxies for $\lambda > 2.2 \mu\text{m}$, slightly dependent on the choice of the upper and lower limits of the count integration. If we consider a constant (**flat** model) contribution of normal galaxies up to 2.2 μm the value of f_* goes from ~ 0.24 ($z_{end} = 8$) to ~ 0.58 ($z_{end} = 10$). The value of f_* decreases considerably if we consider a top-heavy IMF. For the **cut** model of the normal galaxy contribution, f_* ranges between ~ 0.15 ($z_{end} = 8$) and ~ 0.36 ($z_{end} = 10$) if $M_c = 15 M_\odot$ and between ~ 0.1 and ~ 0.23 if $M_c = 100 M_\odot$, whereas for the **flat** model we find f_* values from ~ 0.1 ($z_{end} = 8$) to ~ 0.23 ($z_{end} = 10$) with a heavy IMF, and $\sim 0.06 - 0.15$ (for $z_{end} = 8 - 10$) with a very heavy IMF.

To find the best model, we allow both f_* and z_{end} to vary simultaneously and perform a two-parameter fit to the NIR data. The results are reported in Table 5. Again, quoted errors take into account for statistical uncertainties of the fit. In Fig. 5 we plot the best fit models for the **cut** contribution of normal galaxies. For the **flat** model the star formation efficiencies are significantly lower than in the **cut** case, but the χ^2/DOF remains always greater than 1.9, showing that a low contribution of normal galaxies for $\lambda > 2.2 \mu\text{m}$ is favored by our model. A very remarkable result is the constancy of $z_{end} \approx 8.8$ in the various cases, independent on the IMF or the galaxy contribution model: its value is strongly constrained by the position of the break around 1 μm . The

IMF	galaxy model	f_*	z_{end}
Salpeter	cut	0.53 ± 0.06	8.79 ± 0.10
	flat	0.32 ± 0.04	8.69 ± 0.01
Heavy	cut	0.21 ± 0.02	8.80 ± 0.01
	flat	0.13 ± 0.02	8.75 ± 0.01
Very heavy	cut	0.14 ± 0.01	8.83 ± 0.01
	flat	0.09 ± 0.01	8.79 ± 0.01

Table 5. Best fit values for f_* and z_{end} with different IMFs. The quoted statistical errors are at 95% C.L..

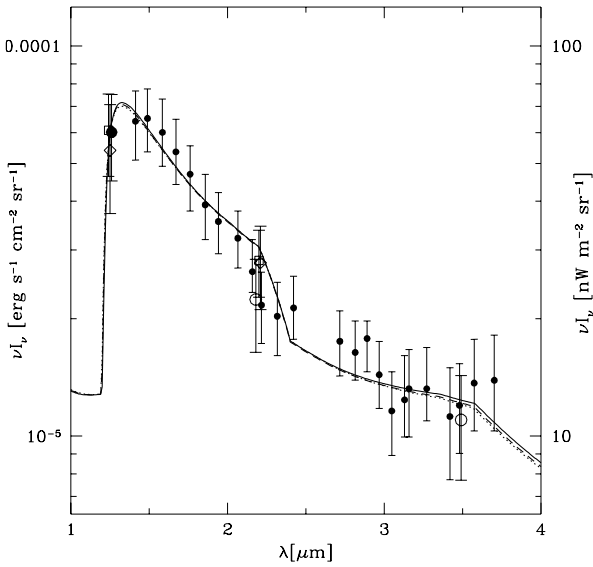


Figure 5. Best results of the fit for different IMFs. *Dashed line:* Salpeter IMF $z_{end} = 8.79$, $f_* = 0.53$. *Dotted line:* heavy IMF $z_{end} = 8.8$, $f_* = 0.21$. *Solid line:* very heavy IMF $z_{end} = 8.82$, $f_* = 0.14$. The model **cut** for the counts integration for $\lambda > 2.2 \mu\text{m}$ is adopted. The data are explained in Sec. 3 and in Fig. 3

break is principally due to the Ly α line emission redshifted into the J band, so that $\lambda_{obs} \sim \lambda_{Ly\alpha}/(1 + z_{end})$.

Barkana (2002) derived a value for f_* using the measured distribution of star formation rates in galaxies at various redshifts (Lanzetta et al. 2002) and semi-analytic models of hierarchical galaxy formation in a Λ CDM cosmology. He found a best fit value of $2.3^{+0.8}_{-0.5}\%$ (2σ), neglecting dust obscuration, but the uncertainties on this evaluation are still large. If this value applies also to the first star formation, for a Salpeter IMF the Pop III contribution to the NIRB is not significant ($< 10\%$), whereas Pop III stars characterized by a top-heavy IMF continue to contribute substantially to the NIRB.

4.2 Associated Metal Enrichment

Recent theoretical analyses on the evolution of metal-free stars predict that the fate of the massive metal-free stars

can be classified as follows (Heger, Woosley & Waters 2000, Chiosi 2000, Heger & Woosley 2002):

(i) $M > 260 M_\odot$: the nuclear energy release from the collapse of stars in this mass range is insufficient to reverse the implosion. The final result is a very massive black hole (VMBH) locking up all heavy elements produced;

(ii) $130 M_\odot < M < 260 M_\odot$: the mass regime of the pair-instability supernovae (SN $_{\gamma\gamma}$). Precollapse winds and pulsations should result in little mass loss, the star implodes reaching a maximum temperature that depends on its mass and then explodes, leaving no remnant. The explosion expels metals into the surrounding ambient ISM;

(iii) $40 M_\odot < M < 130 M_\odot$: black hole formation is the most likely outcome, because either a successful outgoing shock fails to occur or the shock is so weak that the fallback converts the neutron star remnant into a black hole (Fryer 1999);

(iv) $8 M_\odot < M < 40 M_\odot$: SN explosion from ‘normal’ progenitors.

Stars in the mass range (i) and (iii) above fail to eject most of (or all) their heavy elements, whereas (ii) and (iv) type of stars eject metals into the IGM.

To estimate the metal production of Pop III objects we consider SN yields of Woosley & Weaver (1995) for progenitor metal-free stars between 8 and $40 M_\odot$ and the results of Heger & Woosley (2002) for very massive objects of pair instability SNe originating from stars in the mass range $\sim 130 M_\odot$ to $260 M_\odot$. We neglect the contribution from long lived intermediate mass stars ($1 < M < 8 M_\odot$) as their evolution time scale is longer than the Hubble time at the relevant redshift. The density of metals ejected into the IGM in units of the critical density, $\rho_c = 3H_0^2/8\pi G$, is obtained by

$$\Omega_Z(z) = f_Z(\phi) \Omega_*(z) \quad (19)$$

where f_Z is the fraction of metal ejected from normal and pair-instability supernovae; it depends on the adopted IMF, ϕ . Finally, $\Omega_*(z) = \rho_*/\rho_c$, where ρ_* is given in eq. (4).

We calculate the IGM metallicity by imposing that the whole unaccounted NIRB is due to Pop III stars. We use the best results for the efficiency reported in Fig. 5 for the **cut** model of the galaxy counts. We assume here that all the metal escape into the IGM and that they are smoothly distributed. Fig. 6 shows the metallicity of the IGM (in solar units) as a function of redshift.

We compare our results with the estimated value of metals in the Ly α forest ($10^{14.5} < N_{\text{HI}} < 10^{16.5} \text{ cm}^{-2}$) at $z \sim 3$ (Songaila & Cowie 1996; Davé et al. 1998) and in the ‘true’ IGM ($N_{\text{HI}} < 10^{14} \text{ cm}^{-2}$) at $z \sim 5$ (Songaila 2002). Identification of C IV, Si IV and O VI absorption lines which correspond to Ly α absorption lines in the spectra of high redshift quasars has revealed that the low density IGM has been enriched up to $Z_{\text{IGM}} \sim 10^{-2.5 \pm 0.5} Z_\odot$. For lower column density clouds (the ‘true’ IGM) Songaila (2002) found a lower limit on the IGM metallicity at $z \sim 5$ of $10^{-3.5} Z_\odot$.

With the assumed star formation efficiency ($f_* = 0.534$ for a Salpeter; $f_* = 0.214$ for a heavy IMF; $f_* = 0.142$ for a very heavy IMF) the IGM would be enriched to the observed metallicity already at $z = 15 - 18$ for the Ly α forest value and at $z = 20 - 25$ for the ‘true’ IGM lower limit (Fig. 6).

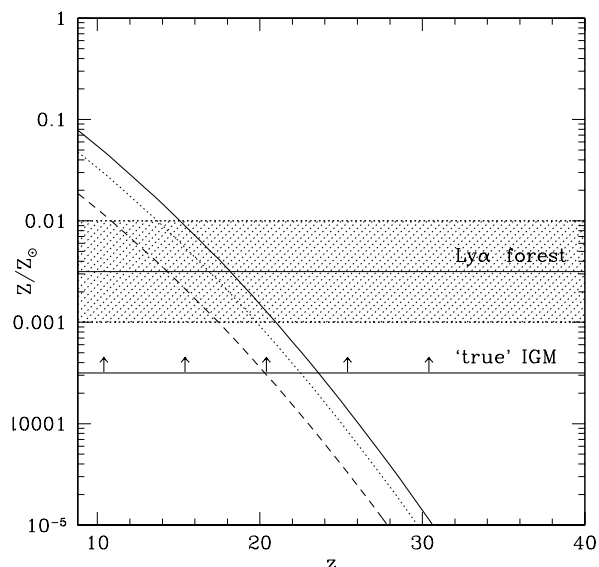


Figure 6. IGM metallicity as a function of redshift. *Dashed line:* Salpeter IMF. *Dotted line:* heavy IMF. *Solid line:* very heavy IMF. The curves are obtained imposing that the whole unaccounted NIRB is due to Pop III stars and the best results for star formation efficiency of Fig. 5 are assumed. The horizontal solid lines represent the value of the metallicity in the Ly α forest (Davé et al. 1998) and in the ‘true’ IGM (Songaila 2002).

As seen from Fig. 6, for $z \sim 8.8$ the mean IGM metallicity exceeds by one order of magnitude that observed in the Ly α forest.

As an alternative, we are thus forced to consider the analogous case in which only pair-instability SNe eject metals into the IGM (Fig. 7). For a Salpeter IMF the obtained metallicity is now consistent with the limits of the Ly α forest, whereas for a heavy IMF this value is slightly exceeded. For top heavy IMFs, for which the contribution of normal SNe is not so important, the results change only slightly.

In order to further reduce these metallicity values, we have to consider lower star formation efficiencies. Consequently only a fraction of the NIRB can be due to Pop III stars. By imposing that Pop III stars do not eject more metals than the observed ones, we find self consistent limits on the star formation efficiency and on the contribution of the first population of stars to the NIRB; Table 6 summarizes the results. Apart for the case of a Salpeter IMF in which only pair-instability SNe contribute to the metal enrichment of the IGM, the star formation efficiency has to be small ($\lesssim 10\%$) and the fraction of NIRB due to Pop III stars is $\lesssim 20\%$.

The value obtained by Songaila (2002) for the ‘true’ IGM at $z \sim 5$ allows us to set a lower limit on the star formation efficiency and the contribution of Pop III stars to the NIRB. The efficiency has to be greater than $\text{few} \times 10^{-4}$ to enrich the IGM to $Z \sim 10^{-3.5} Z_{\odot}$; thus, the Pop III star contribution to the NIRB is at least of the order of 0.4-1.7%. This fraction increases up to 8% if we consider the case in which only pair-instability SNe contribute to the metal enrichment of the universe.

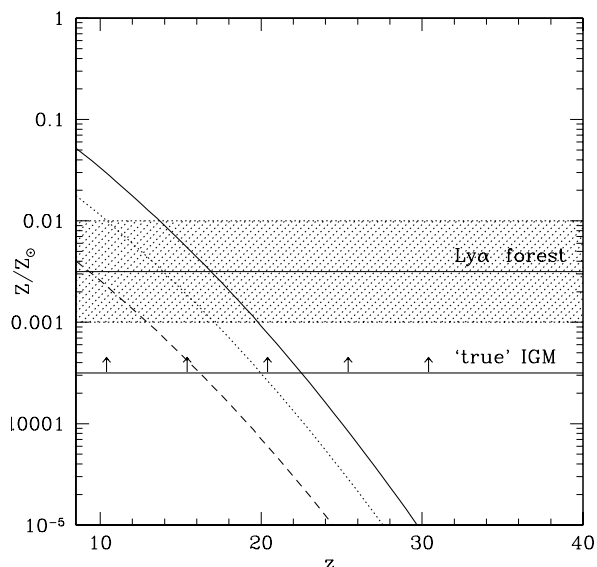


Figure 7. As Fig. 6 but in the case in which only pair-instability SNe eject metals into the IGM. *Dashed line:* Salpeter IMF. *Dotted line:* heavy IMF. *Solid line:* very heavy IMF.

IMF		f_{\star}	% of NIRB
Salpeter	<i>all SN</i>	9.1×10^{-2}	17%
	<i>only SN$_{\gamma\gamma}$</i>	4.3×10^{-1}	80%
Heavy	<i>all SN</i>	1.5×10^{-2}	7%
	<i>only SN$_{\gamma\gamma}$</i>	3.8×10^{-2}	18%
Very Heavy	<i>all SN</i>	0.6×10^{-2}	4%
	<i>only SN$_{\gamma\gamma}$</i>	0.8×10^{-2}	6%

Table 6. The star formation efficiency and the fraction of NIRB from Pop III stars obtained by imposing that metals ejected by Pop III SNe do not exceed the mean observed values in the Ly α forest. The **cut** model for the galaxy counts is assumed.

5 DISCUSSION

Pop III stars can account for the entire NIRB excess if the high redshift star formation efficiency is $f_{\star} = 10\% - 50\%$, depending on the IMF and on the unknown ‘normal’ galaxy contribution in the L band. Our best results are obtained by considering a value $z_{end} \approx 8.8$ for the redshift at which the formation of Pop III stars ends, almost independently of the IMF and of the ‘normal’ galaxy contribution model. A hard upper limit $z_{end} \leq 9$ is set by the J band data. The above efficiency values are not at odd with expectations for objects forming in the Dark Ages (Madau, Ferrara & Rees 2001), although they seem to be higher than those found at lower redshifts.

In addition, the values of f_{\star} found should be considered as upper limits since the unaccounted NIRB level could be lower due to a different zodiacal light subtraction. To quantify this uncertainty we have performed fits using the Wright zodiacal light model. In this case the DIRBE data alone are considered, as NIRS data are only available for the Kelsall model. We find that required star formation efficiencies de-

crease to 0.15 – 0.41 ($z_{end} = 8 - 10$) with a Salpeter IMF, 0.06 – 0.16 with a heavy IMF, and 0.04 – 0.1 with a heavy IMF; at $z_{end} = 8.8$ the resulting star formation efficiencies are 0.23 (Salpeter IMF), 0.09 (heavy IMF), and 0.06 (very heavy IMF). However, the errors are doubled with respect to the case of Kelsall model for the zodiacal light emission. Also, the χ^2 analysis does not allow to evaluate a unique redshift at which Pop III formation ends. This is due to the fact that the break around $1 \mu\text{m}$ is not as sharp as in the previous case, as already mentioned.

As a consistency test, we have calculated the associated IGM metal enrichment. If the whole unaccounted NIRB is due to Pop III stars, then we predict that the low density ('true') IGM would be enriched at the observed mean value already by $z = 15 - 20$, and that the Ly α forest data imply that either a Salpeter or a heavy IMF with characteristic mass $M_c = 15M_\odot$ are acceptable, provided pair-instability SNe are the only source of heavy elements. This conclusion can be modified by the two following occurrences: (i) only stars with masses in excess of $260 M_\odot$ are formed, that lock their nucleosynthetic products into the VMBH remnant, effectively breaking the light-metal production link (Schneider et al. 2002) or (ii) metals are very inhomogeneously mixed in the IGM, with filling factors much smaller than unity (Scannapieco, Ferrara & Madau 2002) at these high redshifts. In both cases, the limits obtained from metallicity arguments are much weaker if not purely indicative.

To exemplify case (i), let us consider an IMF of the form $\phi(M) = \delta(1000 M_\odot)$. By imposing that the whole NIRB is due to Pop III stars ($f_* = 0.04 \pm 0.01$ and $z_{end} = 8.83 \pm 0.01$) and assuming the cut model for the galaxy counts, we obtain a density of VMBH $\Omega_{VMBH}(z = 8.8) \sim 7 \times 10^{-4}$. This value is two orders of magnitude greater than the measured mass density in super massive black holes (SMBHs) found from the demography of nuclei of nearby galaxies (Magorrian et al. 1998; Gebhardt et al. 2001), $\Omega_{SMBH} = 10^{-4} h\Omega_b = 2.66 \times 10^{-6}$ (Merriitt & Ferrarese 2001), but it is unlikely that all VMBHs merge into SMBHs (Schneider et al. 2002; Volonteri, Haardt & Madau 2002). Hence it is not clear if this scenario can represent a viable solution.

In the second case (ii), the measured metallicity might not be representative of the actual cosmic metal density and might result in a large overestimate of the amount of IGM heavy elements. In addition, note that above estimates assume that all the produced heavy elements can escape into the IGM. If the metal escape fraction is equal or less than $\sim 10\%$, the whole unaccounted NIRB could easily be due to Pop III stars with no conflict with the observed IGM metallicity limits.

As a final remark, we point out that additional sources might contribute to the NIRB, as accretion onto black holes (Carr 1994) or decay of massive primordial particles (Bond, Carr & Hogan 1986).

ACKNOWLEDGEMENTS

We thank D. Schaerer for providing Pop III spectra and V. Bromm and L. Danese for constructive and stimulating comments. This work was partially supported (AF) by the Research and Training Network 'The Physics of the Inter-

galactic Medium' set up by the European Community under the contract HPRN-CT2000-00126 RG29185.

REFERENCES

- Abel T., Anninos P.A., Norman M.L., Zhang Y., 1998, ApJ, 508, 518
- Abel T., Bryan G. L., Norman M. L., 2000, ApJ, 540, 39
- Aller L.H., 1987, *Physics of thermal gaseous nebulae*, Astrophysics and space science library, ed. Reidel, Boston
- Arendt R. G., Odegard N., Weiland J. L., Sodroski T. J., Hauser M. G., et al., 1998, ApJ, 508, 74
- Barkana R., 2002, New Astronomy, 7, 337
- Bernstein R. A., Freedman W. L., Madore B. F., 2002, ApJ, 571, 56
- Bond J. R., Carr B. J., Hogan C. J., 1986, ApJ, 306, 428
- Boggess N. W. Mather J. C., Weiss R., Bennett C. L., Cheng, E. S., et al., 1992, ApJ, 397, 420
- Bromm V., Coppi P. S., Larson R. B., 1999, ApJ, 527, L5
- Bromm V., Ferrara, A., Coppi P. S., Larson R. B., 2001, MNRAS, 328, 969
- Bromm V., Coppi P. S., Larson R. B., 2002, ApJ, 564, 23
- Bromm V., Kudritzki R. P., Loeb A., 2001, 552, 464
- Cambrésy L., Reach W. T., Beichman C. A., Jarrett T. H., 2001, ApJ, 555, 563
- Carr B. J., 1994, ARA&A, 32, 531
- Chiosi C., 2000, in *The First Stars*, eds. Weiss A., Abel T., Hill V., Springer, p. 95
- Cohen M., 1997. In *Diffuse Infrared Radiation and the IRST*. ASP Conf. Ser. 124, ed Okura H., Matsumoto T., Roellig T. L., pp. 61-66. San Francisco: Astron. Soc. Pac.
- Cutri R. M., Skrutskie M. F., Van Dyk S., Chester T., Evans T., et al., 2000, *Explanatory Supplement to the 2MASS Second Incremental Data Release*, <http://www.ipac.caltech.edu/2mass/releases/second/doc/explsus.html>
- Davé R., Hellsten U., Hernquist L., Katz N., Weinberg D. H., 1998, ApJ, 509, 661
- Dwek E. & Arendt R. G., 1998, ApJ, 508, L9
- Efstathiou G., Bond J. R., White S. D. M., 1992, MNRAS, 258, 1
- Fardal M. A., Giroux M. L., Shull J. M., 1998, AJ, 115, 2206
- Fryer C. L., 1999, ApJ, 522, 413
- Fuller T. M. & Couchman H. M. P., 2000, ApJ, 544, 6
- Gorjian V., Wright E. L., Chary R. R., 2000, ApJ, 536, 550
- Gebhardt K., Kormendy J, Ho L. C., Bender R., Bower G. et al., 2000, ApJ, 543, L5
- Gnedin N.Y., 2001, submitted to MNRAS (astro-ph/0110290)
- Gunn J. E. & Peterson B. A., 1965, ApJ, 142, 1633
- Haiman Z. & Loeb A., 1999, ApJ, 519, 479
- Hauser M. G., Arendt R. G., Kelsall T., Dwek E., Odegard N., et al., 1998, ApJ, 508, 25
- Hauser M. G. & Dwek E., 2001, ARA&A, 39, 249
- Heger A., Woosley S. L., Waters R., 2000, in *The First Stars*, eds Weiss A., Abel T., Hill V., Springer, p. 121
- Heger A. & Woosley S. E., 2002, ApJ, 567, 532
- Hernandez X. & Ferrara A., 2001, MNRAS, 324, 484
- Kelsall T., Weiland J. L., Franz B. A., Reach W. T., Arendt R. G., et al., 1998, ApJ, 508, 44
- Lanzetta K. M., Yahata N., Pascarella S., Chen H.-W., Fernández-Soto A., 2002, ApJ, 570, 492
- Larson R. B., 1998, MNRAS, 301, 569
- Loeb A. & Rybicki G. B., 1999, ApJ, 524, 527
- Madau P., 1991, ApJ Lett, 376, L33
- Madau P., 1992, ApJ Lett, 389, L1
- Madau P., 1995, ApJ, 441, 18
- Madau P. & Pozzetti L., 2000, MNRAS, 312, L9

- Madau, P., Ferrara, A. & Rees, M. 2001, *ApJ*, 555, 92
- Magorrian J., Tremaine S., Richstone D., Bender R., Bower G. et al., 1998, *AJ*, 115, 2285
- Maihara T., Iwamuro F., Tanabe H., Taguchi T., et al., 2001, *PASJ*, 53, 25
- Mandolesi N., Attolini M. R., Cortiglioni S., Morigi G., Valenziano L., et al., 1998, *A&A*, 331, 463
- Matsumoto T., Cohen M., Freund M. M., Kawaka M., Lim M., et al., 2000, in *ISO Surveys of a Dusty Universe*. Lecture Notes in Physics vol. 548, ed. Lemke D., Stickel M., Wilke K., pp.96-105, Berlin Heidelberg: Springer Verlag
- Merritt D. & Ferrarese L., 2001, *MNRAS*, 320, L30
- Nakamura F. & Umemura M., 2001, *ApJ*, 548, 19
- Noda M., Matsumoto T., Matsuu S., Noguchi K., Tanaka M., et al., 1994, *ApJ*, 428, 363
- Osterbrock D. E., 1989, *Astrophysics of Gaseous Nebulae and Active Galactic Nuclei*, Mill Valley: University Science Book
- Peebles P. J. E., 1993, *Principles of Physical Cosmology*, Princeton Univ. Press, Princeton, NJ
- Press W. H. & Schechter P., 1974, *ApJ*, 187, 425
- Ripamonti, E., Haardt, F., Ferrara, A. & Colpi M., 2002, *MNRAS*, 334, 401
- Salpeter E. E., 1955, *ApJ*, 121, 161
- Santos M. R., Bromm V., Kamionkowski M., 2001, submitted to *MNRAS* (astro-ph/0111467)
- Scannapieco, E., Ferrara, A. & Madau, P. 2002, *ApJ*, 574, 590
- Schaerer D., 2002, *A&A*, 382, 28
- Schneider R., Ferrara A., Natarajan P., Omukai K., 2002, *ApJ*, 571, 30
- Silverberg R. F., Hauser M. G., Boggess N. W., Kelsall T. J., et al., 1993, in *Infrared Spaceborne Remote Sensing*, Proc. SPIE Vol. 2019, ed. Scholl M. S., pp. 180-89, Bellingham: SPIE
- Songaila A., 2002, *ApJ* 568, 139
- Songaila A. & Cowie L. L., 1996, *AJ*, 112, 335
- Totani T., Yoshii Y., Iwamuro F., Maihara T., Motohara K., 2001, *ApJ*, 550, L137
- Tumlinson J. & Shull J. M., 2000, *ApJ*, 528, L65
- Tumlinson J., Giroux M. L., Shull J. M., 2001, *ApJ*, 550, L1
- Volonteri M., Haardt F., Madau P., 2002, submitted to *ApJ* (astro-ph/0207276)
- Wainscoat R. J., Cohen M., Volk K., Walker H. J., Schwartz D. E., 1992, *ApJ Supp.*, 83, 111
- Woosley S. E. & Weaver T. A., 1995, *ApJS*, 101, 181
- Wright E. L., 1998, *ApJ*, 496, 1
- Wright E. L., 2001, *ApJ*, 553, 538
- Wright E. L. & Johnson B. D., 2001, submitted to *ApJ* (astro-ph/0107205)
- Wright E. L. & Reese E. D., 2000, *ApJ*, 545, 43